ACS Sustainable Chemistry & Engineering

pubs.acs.org/journal/ascecg

Research Article

# Recyclable Magnetic MIP-Based SERS Sensors for Selective, Sensitive, and Reliable Detection of Paclobutrazol Residues in Complex Environments

Yichuan Kou, Tong Wu, Hui Zheng, Naveen Reddy Kadasala, Shuo Yang, Chenzi Guo, Lei Chen, Yang Liu,* and Jinghai Yang*

Cite This: *ACS Sustainable Chem. Eng.* 2020, 8, 14549−14556

Read Online

ACCESS | Metrics & More | Article Recommendations | Supporting Information

**ABSTRACT:** In this work, a molecularly imprinted polymer (MIP)-based SERS sensor for selective, sensitive, quantitative, and recyclable detection of paclobutrazol residues in complex environments has been proposed. In this strategy, $Fe_3O_4$@$SiO_2$−Au@Ag (FSAA) nanocomposites with tunable Au@Ag interparticle gaps are constructed. Then, by tuning the Au@Ag nanogaps and investigating the SERS enhancement mechanism of FSAA, we achieve the optimal SERS substrate, FSAA-40. After combining with MIPs, we can selectively detect paclobutrazol in soil with a detection limit of 0.075 μg/g. When the paclobutrazol concentration ranges from 0.075 to 12.75 μg/g, the SERS intensity shows a linear correlation, which opens the possibility for quantitative detection. Our magnetic MIP-based SERS sensor can be easily separated, efficiently recycled, and expanded to more universal environments, which demonstrates a promising future in food and environmental safety.

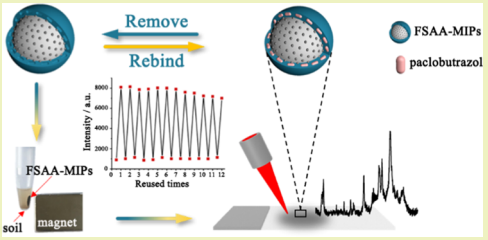


**KEYWORDS:** *SERS, MIPs, magnetic MIP-based SERS sensor, recyclability, paclobutrazol*



## INTRODUCTION

Triazole plant growth regulators, represented by paclobutrazol, play significant roles in reducing vegetative growth and boosting crop yields due to their high efficiency and low toxicity to crops.[1,2] Paclobutrazol has a broad-spectrum bactericidal effect on agronomic and ornamental crops, which can make the stem internodes of crops or plants stout and reduce the lodging risk.[3] Nevertheless, paclobutrazol residues in soil have posed a grave risk to both environmental safety and human health.[4] The excessive use of paclobutrazol can cause a stunting effect on crops and plants.[5] Even if routinely used, paclobutrazol residues can be detected in soil because paclobutrazol is stable and has a fairly long residual period, which not only affects soil microbial activities and growth of crops but also has potential carcinogenicity and genotoxicity to humans.[6]

At present, to evaluate paclobutrazol residues in soil, various methods for determining paclobutrazol were proposed, including high-performance liquid chromatography (HPLC), gas chromatography−mass spectrometry (GC−MS), high-performance liquid chromatography coupled with tandem mass spectrometry (HPLC−MS/MS), and time-resolved fluoroimmunoassay (TRFIA).[1,6−8] However, these detection methods need tedious sample pretreatment processes or expensive advanced instruments, which are incapable of satisfying the green and sustainable chemistry requirements.[9,10] Surface-enhanced Raman scattering (SERS) technology enjoys wide applications in pesticide residue analysis because of its advantages of a nondestructive way of data collection, prominent sensitivity, and rapid detection capability.[11,12] Although SERS is a kind of surface-sensitive analytical technology,[13−18] most studies only focus on the determination of pure pesticide residues on the surfaces of crops or in the aquatic environment.[19,20] The detection of pesticide residues in soil is often overlooked. It is commonly known that the soil composition is far more complex than that on the surfaces of crops or in the aquatic environment. Therefore, it remains a tough challenge to develop an effective method to realize the extraction of paclobutrazol and the quick and selective SERS detection of paclobutrazol in complex environments.

Molecular imprinting technology (MIT) can effectively design biomimetic synthetic receptors for efficient separation of target analytes from complex matrixes.[21−24] Molecularly imprinted polymers (MIPs) synthesized by MIT with good chemical stability, high affinity toward template molecules, and robust molecular recognition ability have attracted comprehensive attention.[25,26] Especially, MIPs have been used as the

Received: July 10, 2020
Revised: August 17, 2020
Published: September 1, 2020

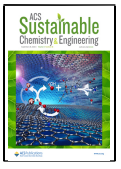




https://dx.doi.org/10.1021/acssuschemeng.0c05065
*ACS Sustainable Chem. Eng.* 2020, 8, 14549−14556

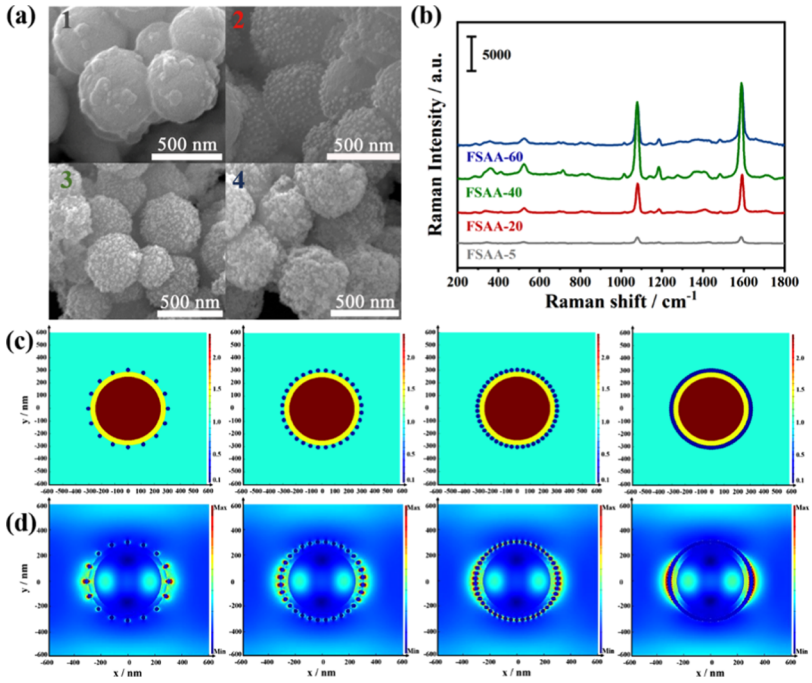


**Figure 1.** SEM images of FSAA-5 (a1), FSAA-20 (a2), FSAA-40 (a3), and FSAA-60 (a4). SERS spectra of 4-MBA adsorbed on FSAA nanocomposites with different additions of Au@Ag nanocrystals (b). FDTD model (c) and the corresponding electric field distribution simulation results (d) with Au@Ag nanocrystals spacings of 60, 16, 12, and 0 nm.

selective adsorbents to apply to the separation, purification, and extraction of trace pesticide residues.[27] Recently, it has become a research hotspot to combine the highly selective recognition ability of MIT with high sensitivity of SERS detection to achieve MIP-based SERS sensors, and research studies have proved their high effectiveness in selectively detecting organic molecules in complex matrixes. For instance, Wang et al. had developed a MIP@Ag NP SERS sensor to selectively and sensitively detect bisphenol A.[28] Zhou et al. had built MIP-AuNPs as a SERS substrate for sensitively and selectively recognizing as well as quantifying L-phenylalanine.[29] Although these studies on MIP-based SERS sensors have been carried out and present excellent SERS properties, surprisingly little attention has been devoted to sensitive SERS detection of paclobutrazol in soil.

Herein, we take advantage of MIPs in targeting selection and develop a magnetic MIP-based SERS sensor for selective, sensitive, quantitative, and recyclable detection of paclobutrazol residues in complex environments. We choose $Fe_3O_4$@$SiO_2$ with auxiliary separation ability and Au@Ag core−shell bimetallic nanocrystals with high SERS performance as magnetic support materials and SERS substrates, respectively. By tuning the spacing between Au@Ag nanocrystals onto the $Fe_3O_4$@$SiO_2$ surfaces, we can obtain the optimal $Fe_3O_4$@$SiO_2$−Au@Ag (FSAA) SERS substrates (i.e., FSAA-40, when the spacing is 12 nm). By combining with finite-difference time-domain (FDTD) simulation results, the SERS enhancement mechanism of FSAA nanocomposites is discussed. After combining the optimal FSAA with MIPs, we can selectively detect paclobutrazol in soil with a detection limit of 0.075 μg/g. In addition, FSAA-MIPs can also be used to detect the paclobutrazol residues on the surfaces of fruits and in the aquatic environment. Our research not only extends the knowledge into the SERS enhancement mechanism of magnetic MIP-based SERS sensors but also opens up novel avenues to design eco-sustainable, versatile, and reusable SERS sensors for selective and sensitive detection of triazole plant growth regulators in complex environments.

## EXPERIMENTAL SECTION

The chemicals and instruments used in this study are presented in the Supporting Information.

**Synthesis of FSAA Nanocomposites.** For the preparation of $Fe_3O_4$@$SiO_2$ core−shell nanocrystals, $Fe_3O_4$ hollow spheres were prepared by applying the same method as in our previous work.[30] Then, an appropriate amount of $Fe_3O_4$ hollow spheres was dispersed in ethanol mixed with deionized water. Subsequently, the mixed solution was added to 4.0 mL of $NH_3{\cdot}H_2O$, 0.8 mL of TEOS, and 1.2 mL of APTES and stirred for 15 h. Finally, the black precipitates of $Fe_3O_4$@$SiO_2$ was washed and dried at 60 °C for later use.

For the preparation of Au@Ag nanocrystals, Au@Ag nanocrystals were synthesized by reducing the Ag shells on the surfaces of Au cores. By applying the same method in our previous work, the Au nanocrystals were prepared.[31] Then, 50 mL of prepared Au nanocrystals was diluted to 200 mL with deionized water before being heated to boiling. Once the boiling point was reached, the solution was immediately added with 1.6 mg/mL $AgNO_3$ and 10 mg/mL $Na_3C_6H_5O_7{\cdot}2H_2O$. The reaction mixture was maintained at 85 °C for 45 min. When the color of the mixture turned to yellow, the Au@Ag nanocrystals were obtained and stored in the dark.

For the preparation of FSAA nanocomposites, 10 mg of as-prepared $Fe_3O_4$@$SiO_2$ nanocrystals were redispersed in 4 mL of deionized water before adding to 5 mL of as-obtained Au@Ag nanocrystals. The mixture was vibrated in a water bath at 40 °C for 10 min. After washing and drying, the obtained sample was named as FSAA-5. With the additional amount of the Au@Ag nanocrystals changed to 20, 40, and 60 mL (5 mL each time), the above experiments were repeated and the FSAA-20, FSAA-40, and FSAA-60 samples were obtained, respectively.

**Synthesis of FSAA-MIPs.** First, KH570 was grafted onto the surfaces of FSAA-40 to obtain FSAA-KH570.[32] Then, 100 mg of FSAA-KH570, 29.3 mg of paclobutrazol, 28.4 mg of AM, 196 μL of EGDMA, and 10 mg of AIBN were dispersed successively in 60 mL of acetonitrile under a $N_2$ atmosphere. The oxygen in the mixture was


https://dx.doi.org/10.1021/acssuschemeng.0c05065
ACS Sustainable Chem. Eng. 2020, 8, 14549−14556

exhausted by purging with $N_2$, and then, the mixture was transferred to a constant-temperature bath oscillator. The mixture was prepolymerized at 50 °C for 5 h and then heated to 60 °C for 25 h. Then, Soxhlet extraction was adapted to extract paclobutrazol (template molecule) from MIPs by utilizing a mixed solution of methanol and acetic acid. Following the same procedures, non-imprinted polymers (FSAA-NIPs) were also achieved.

## RESULTS AND DISCUSSION

**Preparation and Optimization of SERS Substrates.** TEM images of $Fe_3O_4$ hollow spheres, $Fe_3O_4$@$SiO_2$ core–shell nanocrystals, Au nanocrystals, Au@Ag nanocrystals, and FSAA-40 are shown in Figure S1a–e. Figure S1b shows that $Fe_3O_4$ hollow spheres are completely coated by an amorphous $SiO_2$ shell of ~30 nm thickness. As shown in Figure S1f, the UV–vis spectra of Au nanocrystals display a typical surface plasmon resonance (SPR) peak at ~520 nm.[33] By contrast, the prepared Au@Ag nanocrystals exhibit two absorption bands: ~404 and ~714 nm. The peak at ~404 nm is contributed by Ag shells, while the one at ~714 nm can be attributed to the electric interaction between the Au core and Ag shell, which helps prove the formation of bimetallic core–shell Au@Ag nanocrystals.[34,35] Figure S1e shows that Au@Ag nanocrystals are uniformly anchored on the surfaces of $Fe_3O_4$@$SiO_2$ nanocrystals.

We further investigate into the SEM images of FSAA-5, FSAA-20, FSAA-40, and FSAA-60 nanocomposites, as shown in Figure 1a. Nano Measurer 1.2 software is used to measure the interparticle spacings of Au@Ag nanocrystals onto different FSAA samples. As shown in Figure S2, the interparticle spacings of FSAA-5, FSAA-20, FSAA-40, and FSAA-60 are ~60, ~16, ~12 nm, and close to zero, respectively. To compare the SERS performance of different FSAA samples and find out their dependence on the Au@Ag nanocrystal interparticle spacing, we implement 4-MBA as the probe molecule. As presented in Figure 1b, two peaks are observed at 1079 and 1589 $cm^{-1}$, which correspond to the CH in-plane bending vibration and C=C symmetric stretching vibration, respectively.[36] As can be seen, when the spacing between Au@Ag nanocrystals decreases from ~60 nm (FSAA-5) to ~12 nm (FSAA-40), the peak intensity of SERS spectra increases. This is because FSAA-40 has the smallest interparticle spacing and hence has more hotspots and higher hotspot intensity[37,38] compared to FSAA-5 and FSAA-20. However, the SERS intensity of 4-MBA decreases abnormally when FSAA-60 is applied as SERS substrates. A possible explanation is that the excessive agglomeration of Au@Ag nanocrystals or even the formation of a Au@Ag shell has reduced the SERS hotspots and weakened the SERS intensity. FDTD simulations are further employed to verify the relationship between the SERS intensity and the spacing between Au@Ag nanocrystals. The local electric field distributions and intensities of FSAA-5, FSAA-20, FSAA-40, and FSAA-60 are investigated. As shown in Figure 1c,1d, the SERS-active sites are mostly generated around Au@Ag nanocrystals and the electric field enhancement is restricted to gaps between Au@Ag nanocrystals. When the spacing between Au@Ag nanocrystals is 12 nm, the electric field reaches its maximum intensity. Therefore, FSAA-40 proves to be the optimal SERS substrate and is selected for further investigation.

**Construction of Magnetic MIP-Based SERS Sensors.** Figure 2a presents the schematic illustration for the preparation of FSAA-MIPs. The surfaces of FSAA-40 are first

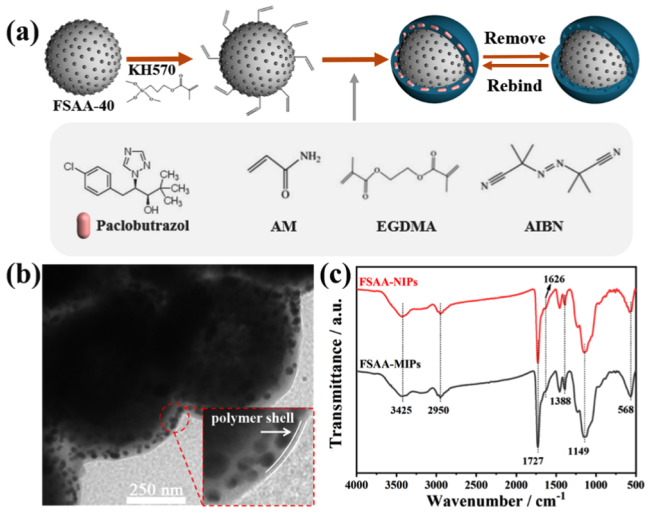


**Figure 2.** Schematic illustration for the preparation of FSAA-MIPs (a), TEM images of FSAA-MIPs (b), and FT-IR spectra of FSAA-MIPs and FSAA-NIPs (c).

modified with vinyl groups, and then, MIPs with specific identification of paclobutrazol are immobilized onto the surface-functionalized FSAA-40. By removing the template molecules via Soxhlet extraction, FSAA-MIP SERS sensors are obtained. TEM results in Figure 2b show that FSAA-40 is uniformly coated with a 15 nm thick MIP layer, which is significantly thinner than ever reported MIP layers and can avoid the decrease of SERS intensity to the largest extent.[39,40] The FT-IR spectra of FSAA-MIPs and FSAA-NIPs are shown in Figure 2c. The two samples show visible bands at similar locations. The peak of Fe–O at 568 $cm^{-1}$ proves the embedding of $Fe_3O_4$ magnetic cores. The characteristic peak at 1388 $cm^{-1}$ is ascribed to the C–N stretching of the functional monomer (AM), and the peaks at 1626 and 3425 $cm^{-1}$ are corresponding to the stretching vibration and bending vibration of secondary amine groups of AM. The absorption peaks at 1149 and 1727 $cm^{-1}$ are ascribed to the C–O–C and C=O stretching of EGDMA. Also, the peak at 2950 $cm^{-1}$ is ascribed to the aliphatic C–H stretching vibrations. The above results indicate that FSAA-MIPs and FSAA-NIPs have been successfully obtained.[39,41]

Template removal from MIPs is indispensable for ensuring the maximum amount of recognition cavities available for the template molecules as much as possible. In fact, complete removal of template molecules from MIPs is almost impossible even after several exhaustive rinsing cycles by conventional Soxhlet extraction.[42] To study the effect of template removal by Soxhlet extraction, SERS spectra of paclobutrazol on FSAA-MIPs after different rinsing times were acquired in Figure S3a, and the Raman spectra of FSAA-NIPs and pure paclobutrazol are given in Figure S4 as a comparison. Density functional theory (DFT) was employed to calculate the vibrational modes of the three main SERS peaks (1007, 1275, and 1397 $cm^{-1}$) of paclobutrazol, as presented in Table S1. It can be noticed that the Raman spectrum of pure paclobutrazol is quite different from the SERS spectra of paclobutrazol on FSAA-MIPs. This may be attributed to the specific interaction between individual vibrational modes and noble metal surfaces.[43] Furthermore, the SERS intensity of paclobutrazol on FSAA-MIPs decreases with the rinsing time. However, even after 3 days rinsing, the template molecules (paclobutrazol) have not been completely


https://dx.doi.org/10.1021/acssuschemeng.0c05065
ACS Sustainable Chem. Eng. 2020, 8, 14549–14556

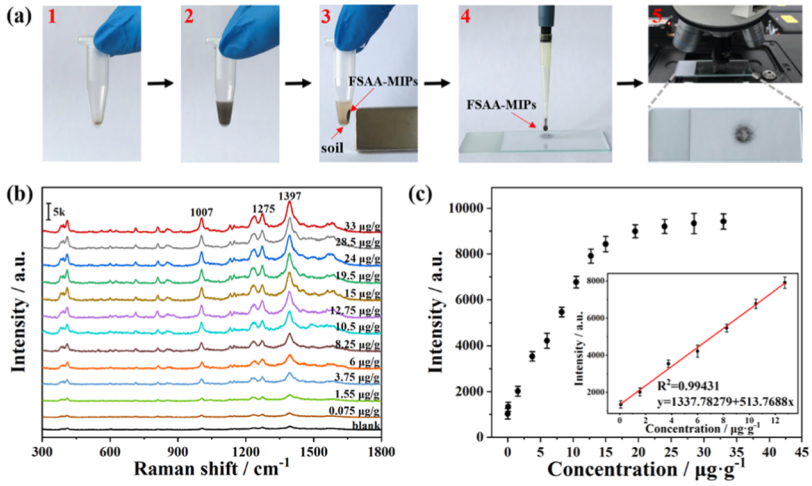


**Figure 3.** SERS detection of paclobutrazol in soil with FSAA-MIPs (a). SERS spectra of various paclobutrazol concentrations in soil (b) and the relationship between the SERS intensity at 1397 $cm^{-1}$ and paclobutrazol concentrations (c).

removed. To exclude the influence of residual template molecules on quantitative determination, FSAA-MIPs after rinsing for 3 days are used as blank samples.[44] The SERS spectra of paclobutrazol from randomly selected 20 points on the blank samples are shown in Figure S3b. The threshold values of the three main peaks at 1007, 1275, and 1397 $cm^{-1}$, calculated from mean intensities plus three times the standard deviation of blank samples, are found to be 609, 905, and 1296, respectively. We hence chose the strongest signal bands located at 1397 $cm^{-1}$ as the reference peak to ensure the data accuracy.

**Application of Magnetic MIP-Based SERS Sensors for SERS Detection of Paclobutrazol in Soil.** Our prepared FSAA-MIP SERS sensors are applied to the detection of paclobutrazol in soil, as presented in Figure 3a. First, the soil samples are obtained from the Nursery Garden of Changchun. The soil sample (20 mg) spiked with paclobutrazol is put into a centrifuge tube. Second, the diluted suspension of FSAA-MIPs is added to the tube and received 2 h of incubation. Third, we separate FSAA-MIPs with an external magnetic field and transfer them to precleaned glass slides, while the soil is remained at the bottom of the tube. Then, a Raman spectrometer is utilized to investigate the SERS spectra of paclobutrazol (under 632.8 nm laser excitation). To rule out the influence of other soil components on the SERS signal intensities of paclobutrazol, we compare the SERS spectra of heat-treated soil samples (heating treatment at 500 °C for 4 h) spiked with paclobutrazol and untreated soil samples spiked with paclobutrazol. As seen in Figure S6, heat treatment shows no influence on the SERS intensities of soil samples. In other words, the other organic soil components have no influence on the SERS signals of paclobutrazol. Figure 3b,3c shows the SERS spectra of paclobutrazol with different concentrations and the relationship between the SERS intensity at 1397 $cm^{-1}$ and paclobutrazol concentrations, respectively. In comparison, the SERS spectrum of FSAA-MIPs after rinsing for 3 days, named as blank, is also presented in Figure 3b. We spike different amounts of paclobutrazol (0.075−34 $\mu$g/g) to the heat-treated soil samples and find that even when 0.075 $\mu$g/g paclobutrazol is added the SERS intensity of paclobutrazol is still higher than the threshold value. Therefore, it is safe to say that the limit of detection (LOD) of FSAA-MIPs can be as low as 75 ng/g. As shown in Figure 3c, the SERS peak intensity (at 1397 $cm^{-1}$) of paclobutrazol increases with the paclobutrazol concentration and shows a slowdown when the paclobutrazol concentration goes beyond 15 $\mu$g/g. The peak intensity at 1397 $cm^{-1}$ is almost linearly related to the paclobutrazol concentration within the range from 0.075 to 12.75 $\mu$g/g. As exhibited in the inset of Figure 3c, the linear correlation coefficient is 0.994. As described in the Supporting Information, the enhancement factor (EF) of FSAA-MIPs for paclobutrazol detection is around $9.57 \times 10^5$. We further compare the LOD and EF of our FSAA-MIPs to previously reported plasmonic nanoparticles, as shown in Table S2. The above results fully demonstrate the ultrahigh sensitivity of FSAA-MIPs to paclobutrazol in soil.

To evaluate the selective detecting ability of our proposed magnetic MIP-based SERS sensors, we bring in several organic pollutants (thiram, malachite green, and methylene blue, which can be commonly found in soil) as the interfering substances. The soil samples are added with paclobutrazol, followed by the interfering substances (15 $\mu$g/g). We then implement the testing method in Figure 3a, and the SERS signals of paclobutrazol, thiram, malachite green, and methylene blue are given as comparison.[45−47] As exhibited in Figure 4, only the characteristic peaks of paclobutrazol in the spiked soil sample can be observed, while no SERS signals of interfering substances are detected, which demonstrates the excellent selective detecting ability of our FSAA-MIPs. By contrast, when FSAA-40 serves as the SERS substrate under the same conditions, SERS signals of all organic pollutants are obvious

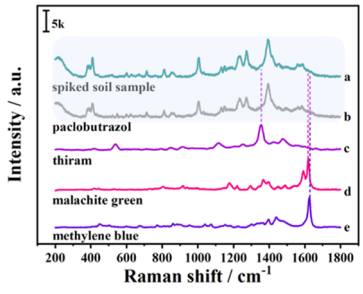


**Figure 4.** SERS spectra of soil sample added with paclobutrazol on FSAA-MIPs (a) and interfering substances of paclobutrazol (b), thiram (c), malachite green (d), and methylene blue (e).



https://dx.doi.org/10.1021/acssuschemeng.0c05065
ACS Sustainable Chem. Eng. 2020, 8, 14549−14556

(Figure S7), which shows no selectivity detection of paclobutrazol. The high selectivity of FSAA-MIPs can be explained by the "key-and-lock" relationship between the template molecules and the MIPs.[48] MIPs with complementary cavities to specific targets ensure that our FSAA-MIPs have high selectivity and strong anti-interference ability toward organic pollutants in soil.[49]

According to the calibration curves in the inset of Figure 3c, we further conduct the spike-and-recovery experiments to assess the accuracy of our method. First, we collect three random soil samples from three farms in Changchun. Then, following the same method in Figure 3a, we add 0.1, 5, and 10 μg/g paclobutrazol to the three soil samples, respectively. As revealed in Table 1, the recoveries of the three soil samples are

**Table 1. Paclobutrazol Recovery in Soil Samples at Three Different Concentrations**

| sample | true value (μg/g) | predicted value (μg/g) | recovery (%) | RSD (%, $n$ = 3) |
|---|---|---|---|---|
| 1 | 0.1 | 0.104 | 104 | 3.67 |
| | 5 | 4.895 | 97.9 | 1.21 |
| | 10 | 9.68 | 96.8 | 4.44 |
| 2 | 0.1 | 0.092 | 92 | 2.01 |
| | 5 | 4.998 | 99.96 | 2.16 |
| | 10 | 11.043 | 110.43 | 5.01 |
| 3 | 0.1 | 0.091 | 91 | 2.65 |
| | 5 | 5.015 | 100.3 | 2.77 |
| | 10 | 10.19 | 101.9 | 4.93 |

96.8−104, 92−110.43, and 91−101.9%, respectively. Also, the coefficients of variation are in the ranges of 1.21−4.44, 2.01−5.01, and 2.65−4.93%, respectively. From our obtained results, one can conclude that our proposed method is effective and credible, which shows the practical promise in detecting the organic pollutant residues in soil.

**Universal Applicability of Magnetic MIP-Based SERS Sensors.** Our magnetic MIP-based SERS sensors can also be expanded to detect the residual paclobutrazol in other environments, e.g., peels of fruits and aquatic environments.[2,6] To demonstrate this universal applicability, we obtained a mango from the local market and obtain some water samples from the local Songhua River. Then, as shown in Figure 5a, 20 mg/L paclobutrazol solution is sprayed on the peels of mango and the diluted suspension of FSAA-MIPs is smeared uniformly on the surfaces of mango peels. After complete evaporation of FSAA-MIPs and air drying, FSAA-MIPs are transferred from the mango peels to a clean glass slide under the external magnetic field. We then implement the transferred FSAA-MIPs for SERS detection, and the result is shown in Figure 5b. As for the water sample, a 0.2 μm aperture membrane was used to filter the collected water samples for removing the insoluble particles.[50,51] Paclobutrazol was added into the collected water sample to make the final concentration of 20 mg/L. The following detection process obeys the method in Figure 3a. As presented in Figure 5c, the characteristic bands of paclobutrazol can be clearly observed. The above results demonstrate the universal applicability of our FSAA-MIPs in detecting paclobutrazol from different and complex environments.

**Reusability and Stability of Magnetic MIP-Based SERS Sensors.** Further, we investigate the reusability and stability of our magnetic MIP-based SERS sensors. With the superparamagnetic $Fe_3O_4$ hollow spheres, our FSAA-MIPs could be easily separated assisted by an external magnetic field.[52] As shown in Figure 6a, the magnetic hysteresis loops of $Fe_3O_4$ and FSAA-MIPs exhibit superparamagnetic characteristics, while their coercivity and remanence can be negligible at 300 K. The saturation magnetization values of $Fe_3O_4$ and FSAA-MIPs are 90 and 39 emu/g, respectively. Compared to $Fe_3O_4$ hollow spheres, the saturation magnetization of FSAA-MIPs is compromised due to the surface coatings of Au@Ag, $SiO_2$, and MIP, but it is still sufficient to achieve a rapid response to the external magnetic field, as shown in the inset of Figure 6a. After removing the paclobutrazol from FSAA-MIPs by Soxhlet extraction, the sequential adsorption−desorption experiments are repeated 12 times to assess the reusability of FSAA-MIPs. As can be seen from Figure 6b, the adsorption ability of FSAA-MIPs presents a slight decline but still proves great recyclability. Then, 10 samples are prepared, applied to paclobutrazol detection, and kept under the exact same conditions. As presented in Figure 6c, the SERS intensity of

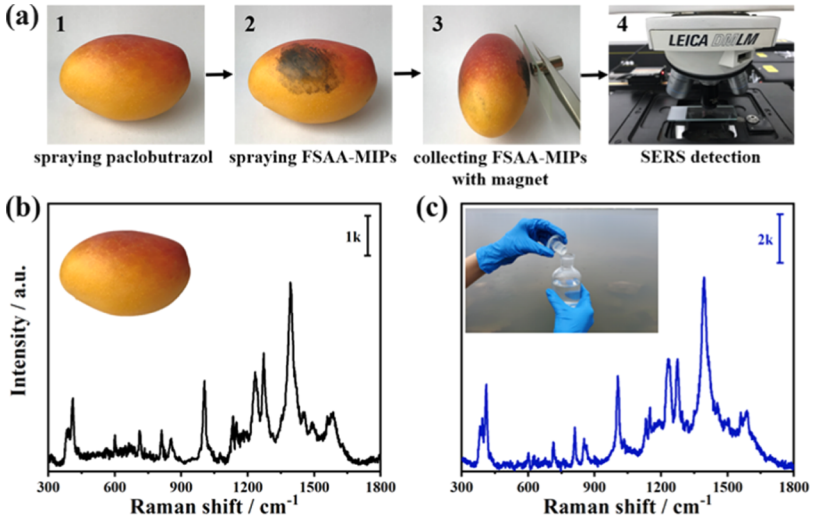


**Figure 5.** SERS detection of paclobutrazol on mango peel by FSAA-MIPs (a). SERS spectra of paclobutrazol on mango peel (b) and in water samples (c).



https://dx.doi.org/10.1021/acssuschemeng.0c05065
ACS Sustainable Chem. Eng. 2020, 8, 14549−14556

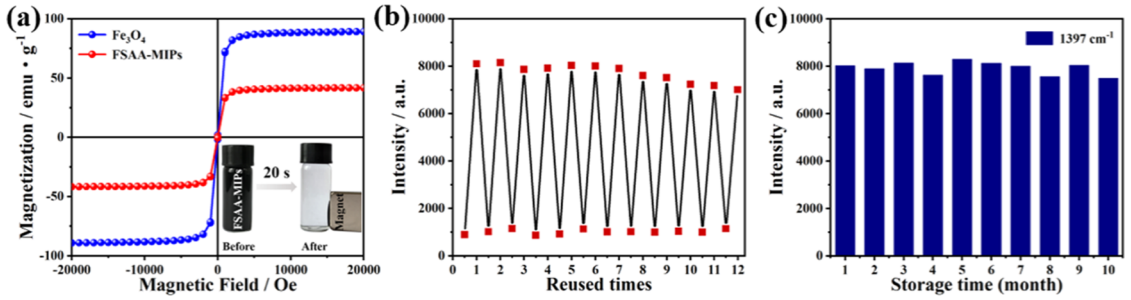


**Figure 6.** Magnetic hysteresis loops of $Fe_3O_4$ and FSAA-MIPs (a), adsorption−desorption cycles of FSAA-MIPs (b), and SERS intensity distribution histograms around 1397 $cm^{-1}$ with different storage times (c). The inset of (a) is the photograph of FSAA-MIPs before and after magnetic separation.

paclobutrazol remains almost unchanged through even after 10 months of storage. These results demonstrate the excellent reusability and stability of our magnetic MIP-based SERS sensors.

## CONCLUSIONS

In summary, we develop a new magnetic FSAA-MIP SERS sensor, which can realize selective, sensitive, quantitative, and recyclable detection of paclobutrazol residues in complex environments. By tuning the spacing between Au@Ag nanocrystals onto the $Fe_3O_4$@$SiO_2$ surfaces, we can obtain the optimal FSAA SERS substrates (i.e., FSAA-40, when the spacing is 12 nm). The SERS enhancement mechanism of FSAA nanocomposites is discussed. Then, by combining the optimal FSAA with MIPs, we are able to selectively detect the paclobutrazol in soil. The limit of detection is as low as 0.075 $\mu$g/g and when the paclobutrazol concentration ranges from 0.075 to 12.75 $\mu$g/g, the SERS intensity shows a linear correlation to the paclobutrazol concentration, which could be applied to the quantitative detection of paclobutrazol. We then demonstrate that the proposed FSAA-MIPs can be expanded to more universal applications and can be easily separated and efficiently reused. Our research offers a novel avenue for the recyclable SERS detection of pesticide residues with high sensitivity and selectivity in the fields of food and environmental safety.

## ASSOCIATED CONTENT

### Supporting Information

The Supporting Information is available free of charge at https://pubs.acs.org/doi/10.1021/acssuschemeng.0c05065.

Chemicals and instruments of experiments, TEM images, UV−vis spectra of Au and Au@Ag nanocrystals, histogram of spacing distribution between Au@Ag nanocrystals on $Fe_3O_4$@$SiO_2$ core−shell nanocrystal surfaces, SERS spectra of paclobutrazol on FSAA-MIPs after removing template molecules, SERS spectra of paclobutrazol from randomly selected 20 points on FSAA-MIPs after removing template molecules, Raman spectra of FSAA-NIPs and paclobutrazol, optimized geometry of paclobutrazol molecule, Raman and DFT-scaled calculated spectra of paclobutrazol, SERS spectra of calcinated and real soil samples added with paclobutrazol, and SERS spectra of the soil sample spiked with paclobutrazol as well as interfering substances on FSAA-40 (PDF)

## AUTHOR INFORMATION


### Corresponding Authors

**Yang Liu** − *College of Physics, Jilin Normal University, Siping 136000, P. R. China;* orcid.org/0000-0003-1485-8764; Email: liuyang@jlnu.edu.cn

**Jinghai Yang** − *College of Physics, Jilin Normal University, Siping 136000, P. R. China;* orcid.org/0000-0001-8409-6035; Email: jhyang1@jlnu.edu.cn

### Authors

**Yichuan Kou** − *College of Physics, Jilin Normal University, Siping 136000, P. R. China*

**Tong Wu** − *College of Physics, Jilin Normal University, Siping 136000, P. R. China*

**Hui Zheng** − *College of Physics, Jilin Normal University, Siping 136000, P. R. China*

**Naveen Reddy Kadasala** − *Department of Chemistry, Towson University, Towson, Maryland 21252, United States*

**Shuo Yang** − *Changchun Institute of Optics, Fine Mechanics and Physics, Chinese Academy of Sciences, Changchun 130033, P. R. China*

**Chenzi Guo** − *Changchun Institute of Optics, Fine Mechanics and Physics, Chinese Academy of Sciences, Changchun 130033, P. R. China*

**Lei Chen** − *College of Physics, Jilin Normal University, Siping 136000, P. R. China;* orcid.org/0000-0003-2616-2190

Complete contact information is available at: https://pubs.acs.org/10.1021/acssuschemeng.0c05065


### Notes

The authors declare no competing financial interest.

## ACKNOWLEDGMENTS

This work was financed by the National Natural Science Foundation of China (Nos. 21676115, 61675090, and 61705020), the Program for Development of Science and Technology of Jilin Province (Nos. 20200301043RQ and 20190103002JH), and the Program for Science and Technology of Education Department of Jilin Province (Nos. JJKH20200418KJ, JJKH20191022KJ, and JJKH20190550KJ).

## REFERENCES

(1) Wu, C.; Sun, J.; Zhang, A.; Liu, W. Dissipation and enantioselective degradation of plant growth retardants paclobutrazol and uniconazole in open field, greenhouse, and laboratory soils. *Environ. Sci. Technol.* **2013**, *47*, 843−849.

(2) Singh, V. K.; Bhattacherjee, A. K. Genotypic response of mango yield to persistence of paclobutrazol in soil. *Sci. Hortic.* **2005**, *106*, 53−59.
(3) Jacyna, T.; Dodds, K. G. Some effects of soil-applied paclobutrazol on performance of 'Sundrop' apricot (*Prunus armeniaca* L.) trees and on residue in the soil. *N. Z. J. Crop Hortic. Sci.* **1995**, *23*, 323−329.
(4) Zhang, C. H.; Zhu, J.; Li, J. J.; Zhao, J. W. Small and sharp triangular silver nanoplates synthesized utilizing tiny triangular nuclei and their excellent SERS activity for selective detection of thiram residue in soil. *ACS Appl. Mater. Interfaces* **2017**, *9*, 17387−17398.
(5) Silva, C. M. M. S.; Vieira, R. F.; Nicolella, G. Paclobutrazol effects on soil microorganisms. *Appl. Soil Ecol.* **2003**, *22*, 79−86.
(6) Liu, Z.; Wei, X.; Ren, K.; Zhu, G.; Zhang, Z.; Wang, J.; Du, D. Highly efficient detection of paclobutrazol in environmental water and soil samples by time-resolved fluoroimmunoassay. *Sci. Total Environ.* **2016**, *569−570*, 1629−1634.
(7) Sharma, D.; Awasthi, M. D. Uptake of soil applied paclobutrazol in mango (*Mangifera indica* L.) and its persistence in fruit and soil. *Chemosphere* **2005**, *60*, 164−169.
(8) Luo, Z.; Zhang, L.; Mou, Y.; Cui, S.; Gu, Z.; Yu, J.; Ma, X. Multi-residue analysis of plant growth regulators and pesticides in traditional Chinese medicines by high-performance liquid chromatography coupled with tandem mass spectrometry. *Anal. Bioanal. Chem.* **2019**, *411*, 2447−2460.
(9) Viveiros, R.; Bonifácio, V. D. B.; Heggie, W.; Casimiro, T. Green development of polymeric dummy artificial receptors with affinity for amide-based pharmaceutical impurities. *ACS Sustainable Chem. Eng.* **2019**, *7*, 15445−15451.
(10) Zhang, Y.; Tan, X.; Liu, X.; Li, C.; Zeng, S.; Wang, H.; Zhang, S. Fabrication of multilayered molecularly imprinted membrane for selective recognition and separation of artemisinin. *ACS Sustainable Chem. Eng.* **2019**, *7*, 3127−3137.
(11) Jiang, J.; Zou, S.; Ma, L.; Wang, S.; Liao, J.; Zhang, Z. Surface-enhanced Raman scattering detection of pesticide residues using transparent adhesive tapes and coated silver nanorods. *ACS Appl. Mater. Interfaces* **2018**, *10*, 9129−9135.
(12) Han, D.; Li, B.; Chen, Y.; Wu, T.; Kou, Y.; Xue, X.; Chen, L.; Liu, Y.; Duan, Q. Facile synthesis of Fe3O4@Au core-shell nanocomposite as a recyclable magnetic surface enhanced Raman scattering substrate for thiram detection. *Nanotechnology* **2019**, *30*, No. 465703.
(13) Li, D.; Cao, X.; Zhang, Q.; Ren, X.; Jiang, L.; Li, D.; Deng, W.; Liu, H. Facile in situ synthesis of core−shell MOF@Ag nanoparticle composites on screen-printed electrodes for ultrasensitive SERS detection of polycyclic aromatic hydrocarbons. *J. Mater. Chem. A* **2019**, *7*, 14108−14117.
(14) Zhu, Z.; Bai, B.; You, O.; Li, Q.; Fan, S. Fano resonance boosted cascaded optical field enhancement in a plasmonic nanoparticle-in-cavity nanoantenna array and its SERS application. *Light: Sci. Appl.* **2015**, *4*, No. e296.
(15) Huang, Y.; Fang, Y.; Zhang, Z.; Zhu, L.; Sun, M. Nanowire-supported plasmonic waveguide for remote excitation of surface-enhanced Raman scattering. *Light: Sci. Appl.* **2014**, *3*, No. e199.
(16) Dai, Z.; Xiao, X.; Wu, W.; Zhang, Y.; Liao, L.; Guo, S.; Ying, J.; Shan, C.; Sun, M.; Jiang, C. Plasmon-driven reaction controlled by the number of graphene layers and localized surface plasmon distribution during optical excitation. *Light: Sci. Appl.* **2015**, *4*, No. e342.
(17) Dong, H.; Yao, D.; Zhou, Q.; Zhang, L.; Tian, Y. An integrated platform for the capture of circulating tumor cells and in situ SERS profiling of membrane proteins through rational spatial organization of multi-functional cyclic RGD nanopatterns. *Chem. Commun.* **2019**, *55*, 1730−1733.
(18) Yang, S.; Yao, J. C.; Quan, Y. N.; Hu, M. Y.; Su, R.; Gao, M.; Han, D. L.; Yang, J. H. Monitoring the charge transfer process in a Nd-doped semiconductor based on photoluminescence and SERS technology. *Light: Sci. Appl.* **2020**, 1−7.
(19) Yao, J.; Quan, Y.; Gao, M.; Gao, R.; Chen, L.; Liu, Y.; Lang, J.; Shen, H.; Zhang, Y.; Yang, L.; Yang, J. AgNPs decorated Mg-doped ZnO heterostructure with dramatic SERS activity for trace detection of food contaminants. *J. Mater. Chem. C* **2019**, *7*, 8199−8208.
(20) Quan, Y.; Yao, J.; Yang, S.; Chen, L.; Liu, Y.; Lang, J.; Zeng, H.; Yang, J.; Gao, M. Detect, remove and re-use: Sensing and degradation pesticides via 3D tilted ZMRs/Ag arrays. *J. Hazard. Mater.* **2020**, *391*, No. 122222.
(21) Pan, J.; Chen, W.; Ma, Y.; Pan, G. Molecularly imprinted polymers as receptor mimics for selective cell recognition. *Chem. Soc. Rev.* **2018**, *47*, 5574−5587.
(22) Arabi, M.; Ghaedi, M.; Ostovan, A. Development of a lower toxic approach based on green synthesis of water-compatible molecularly imprinted nanoparticles for the extraction of hydrochlorothiazide from human urine. *ACS Sustainable Chem. Eng.* **2017**, *5*, 3775−3785.
(23) López-Porfiri, P.; Gorgojo, P.; Gonzalez-Miquel, M. Green solvent selection guide for biobased organic acid recovery. *ACS Sustainable Chem. Eng.* **2020**, *8*, 8958−8969.
(24) Yang, Z.; Chen, J.; Wang, J.; Zhang, Q.; Zhang, B. Self-driven BSA surface imprinted magnetic tubular carbon nanofibers: fabrication and adsorption performance. *ACS Sustainable Chem. Eng.* **2020**, *8*, 3241−3252.
(25) Ostovan, A.; Ghaedi, M.; Arabi, M.; Yang, Q.; Li, J.; Chen, L. Hydrophilic multitemplate molecularly imprinted biopolymers based on a green synthesis strategy for determination of B-family vitamins. *ACS Appl. Mater. Interfaces* **2018**, *10*, 4140−4150.
(26) Gui, R.; Jin, H.; Guo, H.; Wang, Z. Recent advances and future prospects in molecularly imprinted polymers-based electrochemical biosensors. *Biosens. Bioelectron.* **2018**, *100*, 56−70.
(27) Zhao, B.; Feng, S.; Hu, Y.; Wang, S.; Lu, X. Rapid determination of atrazine in apple juice using molecularly imprinted polymers coupled with gold nanoparticles-colorimetric/SERS dual chemosensor. *Food Chem.* **2019**, *276*, 366−375.
(28) Wang, Z.; Yan, R.; Liao, S.; Miao, Y.; Zhang, B.; Wang, F.; Yang, H. In situ reduced silver nanoparticles embedded molecularly imprinted reusable sensor for selective and sensitive SERS detection of Bisphenol A. *Appl. Surf. Sci.* **2018**, *457*, 323−331.
(29) Zhou, J.; Sheth, S.; Zhou, H.; Song, Q. Highly selective detection of L-Phenylalanine by molecularly imprinted polymers coated Au nanoparticles via surface-enhanced Raman scattering. *Talanta* **2020**, *211*, No. 120745.
(30) Chen, Y.; Zhang, Y.; Kou, Q.; Liu, Y.; Han, D.; Wang, D.; Sun, Y.; Zhang, Y.; Wang, Y.; Lu, Z.; Chen, L.; Yang, J.; Xing, S. G. Enhanced catalytic reduction of 4-nitrophenol driven by Fe3O4-Au magnetic nanocomposite interface engineering: from facile preparation to recyclable application. *Nanomaterials* **2018**, *8*, No. 353.
(31) Wu, T.; Kou, Y.; Zheng, H.; Lu, J.; Kadasala, N. R.; Yang, S.; Guo, C.; Liu, Y.; Gao, M. A novel Au@Cu2O-Ag ternary nanocomposite with highly efficient catalytic performance: towards rapid reduction of methyl orange under dark condition. *Nanomaterials* **2020**, *10*, No. 48.
(32) Li, H.; Wang, X.; Wang, Z.; Jiang, J.; Wei, M.; Zheng, J.; Yan, Y.; Li, C. Thermo-responsive molecularly imprinted sensor based on the surface-enhanced Raman scattering for selective detection of R6G in the water. *Dalton Trans.* **2017**, *46*, 11282−11290.
(33) Liu, Y.; Zhang, Y. Y.; Kou, Q. W.; Wang, D. D.; Han, D. L.; Lu, Z. Y.; Chen, Y.; Chen, L.; Wang, Y. X.; Zhang, Y. J.; Yang, J. H.; Xing, S. Fe3O4/Au binary nanocrystals: Facile synthesis with diverse structure evolution and highly efficient catalytic reduction with cyclability characteristics in 4-nitrophenol. *Powder Technol.* **2018**, *338*, 26−35.
(34) Majhi, J. K.; Kuiri, P. K. Enhancement of spectral shift of plasmon resonances in bimetallic noble metal nanoparticles in core−shell structure. *J. Nanopart. Res.* **2020**, *22*, 1−12.
(35) Rai, P.; Khan, R.; Raj, S.; Majhi, S. M.; Park, K. K.; Yu, Y. T.; Lee, I. H.; Sekhar, P. K. Au@Cu2O core-shell nanoparticles as chemiresistors for gas sensor applications: effect of potential barrier modulation on the sensing performance. *Nanoscale* **2014**, *6*, 581−588.
(36) Han, B.; Ma, N.; Yu, J.; Xiao, L.; Guo, S.; Park, E.; Jin, S.; Chen, L.; Jung, Y. M. Probing the charge-transfer of Ag/PEDOT:PSS/4-


https://dx.doi.org/10.1021/acssuschemeng.0c05065
*ACS Sustainable Chem. Eng.* 2020, 8, 14549−14556

MBA by surface-enhanced raman scattering. *Spectrochim. Acta, Part A* **2020**, *239*, No. 118451.
(37) Ding, S. Y.; You, E. M.; Tian, Z. Q.; Moskovits, M. Electromagnetic theories of surface-enhanced Raman spectroscopy. *Chem. Soc. Rev.* **2017**, *46*, 4042−4076.
(38) Gao, R.; Zhang, Y.; Zhang, F.; Guo, S.; Wang, Y.; Chen, L.; Yang, J. SERS polarization-dependent effects for an ordered 3D plasmonic tilted silver nanorod array. *Nanoscale* **2018**, *10*, 8106−8114.
(39) Wang, Y.; Li, H.; Wang, X.; Wang, Z.; Wang, M.; Li, Y.; Wang, Q. Preparation of a high-performance magnetic molecularly imprinted sensor for SERS detection of cyfluthrin in river. *J. Raman Spectrosc.* **2019**, 926−935.
(40) Li, H.; Jiang, J.; Wang, Z.; Wang, X.; Liu, X.; Yan, Y.; Li, C. A high performance and highly-controllable core-shell imprinted sensor based on the surface-enhanced Raman scattering for detection of R6G in water. *J. Colloid Interface Sci.* **2017**, *501*, 86−93.
(41) Li, H.; Wang, Z.; Wang, X.; Jiang, J.; Xu, Y.; Liu, X.; Yan, Y.; Li, C. Preparation of a self-cleanable molecularly imprinted sensor based on surface-enhanced Raman spectroscopy for selective detection of R6G. *Anal. Bioanal. Chem.* **2017**, *409*, 4627−4635.
(42) Lorenzo, R. A.; Carro, A. M.; Alvarez-Lorenzo, C.; Concheiro, A. To remove or not to remove? The challenge of extracting the template to make the cavities available in molecularly imprinted polymers (MIPs). *Int. J. Mol. Sci.* **2011**, *12*, 4327−4347.
(43) Li, H.; Yue, X.; Gao, N.; Tang, J.; Lv, X.; Hou, J. Microwave method synthesis of magnetic ionic liquid/gold nanoparticles as ultrasensitive SERS substrates for trace clopidol detection. *Anal. Bioanal. Chem.* **2020**, *412*, 3063−3071.
(44) Cong, F.; Zhu, Y.; Wang, J.; Lian, Y.; Liu, X.; Xiao, L.; Huang, R.; Zhang, Y.; Chen, M.; Guo, P. A multiplex xTAG assay for the simultaneous detection of five chicken immunosuppressive viruses. *BMC Vet. Res.* **2018**, *14*, 347.
(45) Hussain, A.; Sun, D. W.; Pu, H. Bimetallic core shelled nanoparticles (Au@AgNPs) for rapid detection of thiram and dicyandiamide contaminants in liquid milk using SERS. *Food Chem.* **2020**, *317*, No. 126429.
(46) Lin, S.; Hasi, W.; Lin, X.; Han, S.; Xiang, T.; Liang, S.; Wang, L. Lab-on-capillary platform for on-site quantitative SERS analysis of surface contaminants based on Au@4-MBA@Ag core-shell nanorods. *ACS Sens.* **2020**, *5*, 1465−1473.
(47) Demirel, G.; Gieseking, R. L. M.; Ozdemir, R.; Kahmann, S.; Loi, M. A.; Schatz, G. C.; Facchetti, A.; Usta, H. Molecular engineering of organic semiconductors enables noble metal-comparable SERS enhancement and sensitivity. *Nat. Commun.* **2019**, *10*, No. 5502.
(48) Kamra, T.; Zhou, T.; Montelius, L.; Schnadt, J.; Ye, L. Implementation of molecularly imprinted polymer beads for surface enhanced Raman detection. *Anal. Chem.* **2015**, *87*, 5056−5061.
(49) Hu, Y.; Feng, S.; Gao, F.; Li-Chan, E. C.; Grant, E.; Lu, X. Detection of melamine in milk using molecularly imprinted polymers-surface enhanced Raman spectroscopy. *Food Chem.* **2015**, *176*, 123−129.
(50) Zengin, A.; Tamer, U.; Caykara, T. Extremely sensitive sandwich assay of kanamycin using surface-enhanced Raman scattering of 2-mercaptobenzothiazole labeled gold@silver nanoparticles. *Anal. Chim. Acta* **2014**, *817*, 33−41.
(51) Li, H.; Wang, X.; Wang, Z.; Jiang, J.; Qiao, Y.; Wei, M.; Yan, Y.; Li, C. A high-performance SERS-imprinted sensor doped with silver particles of different surface morphologies for selective detection of pyrethroids in rivers. *New J. Chem.* **2017**, *41*, 14342−14350.
(52) Zhang, Y.; Liu, D.; Peng, J.; Cui, Y.; Shi, Y.; He, H. Magnetic hyperbranched molecularly imprinted polymers for selective enrichment and determination of zearalenone in wheat proceeded by HPLC-DAD analysis. *Talanta* **2020**, *209*, No. 120555.


https://dx.doi.org/10.1021/acssuschemeng.0c05065
*ACS Sustainable Chem. Eng.* 2020, 8, 14549−14556